ASSOCIATED CONTENT

α/β-Ni(OH)$_2$ Phase Control by F-ion Incorporation to Optimise Hybrid Supercapacitor Performance

Xuerui Yi [a], Veronica Celorrio [b], Haoyu Zhang [a], Neil Robertson[a*] and Caroline Kirk[a*]

a. School of Chemistry and EaStCHEM, University of Edinburgh, King's Buildings, David Brewster Road, Edinburgh, Scotland EH9 3FJ, UK.

b. Diamond Light Source Ltd, Harwell Science and Innovation Campus, Oxfordshire, Didcot, OX11 0DE, UK.

Label	Additive	Molar ratio of additive: Ni(NO$_3$)$_2$	Temperature	Time	Mass of Ni(OH)$_2$ attached for three-electrodes test (mg/cm^2)
α-Ni(OH)$_2$	No additive	0:2	200	5h	2.8
αβ_1-Ni(OH)$_2$	NH_4F	0.2:2			2.1
αβ_2-Ni(OH)$_2$	NH_4F	0.5:2			3.0
β_1-Ni(OH)$_2$ (β-Ni(OH)$_2$)	NH_4F	1:2			2.2
β_2-Ni(OH)$_2$	NH_4F	4:2			
αβ_1-Ni(OH)$_2$_NaF	NaF	0.2:2			
αβ_2-Ni(OH)$_2$_NaF	NaF	0.5:2			
β_1-Ni(OH)$_2$_NaF	NaF	1:2			
β_2-Ni(OH)$_2$_NaF	NaF	4:2			
α_1-Ni(OH)$_2$_NH_4Cl	NH_4Cl	0.2:2			
α_2-Ni(OH)$_2$_NH_4Cl	NH_4Cl	0.5:2			
α_3-Ni(OH)$_2$_NH_4Cl	NH_4Cl	1:2			

Table S1. All samples prepared under different experimental conditions.

	ICDD-38-715 (space group R-3m)	ICDD-14-117 (space group P-3m1)	α-$Ni(OH)_2$	αβ_1-$Ni(OH)_2$	αβ_2-$Ni(OH)_2$	β-$Ni(OH)_2$
Alpha phase (Å)	*a* = 3.080 *c* =23.41		*a*=3.110 (2) *c*=21.41 (2)	*a*=3.069 (1) *c*=22.051 (4)	*a*= 3.057(1) *c*=22.065(8)	
Beta phase (Å)		*a*=3.126 *c*=4.605		*a*=3.1082(2) *c*=4.5941(9)	*a*=3.1091(2) *c*=4.5937(5)	*a*=3.1032(6) *c*=4.5869(7)

Table S2. Refined unit cell parameters of nickel hydroxides after refinement of PXRD data using a Pawley fitting routine.

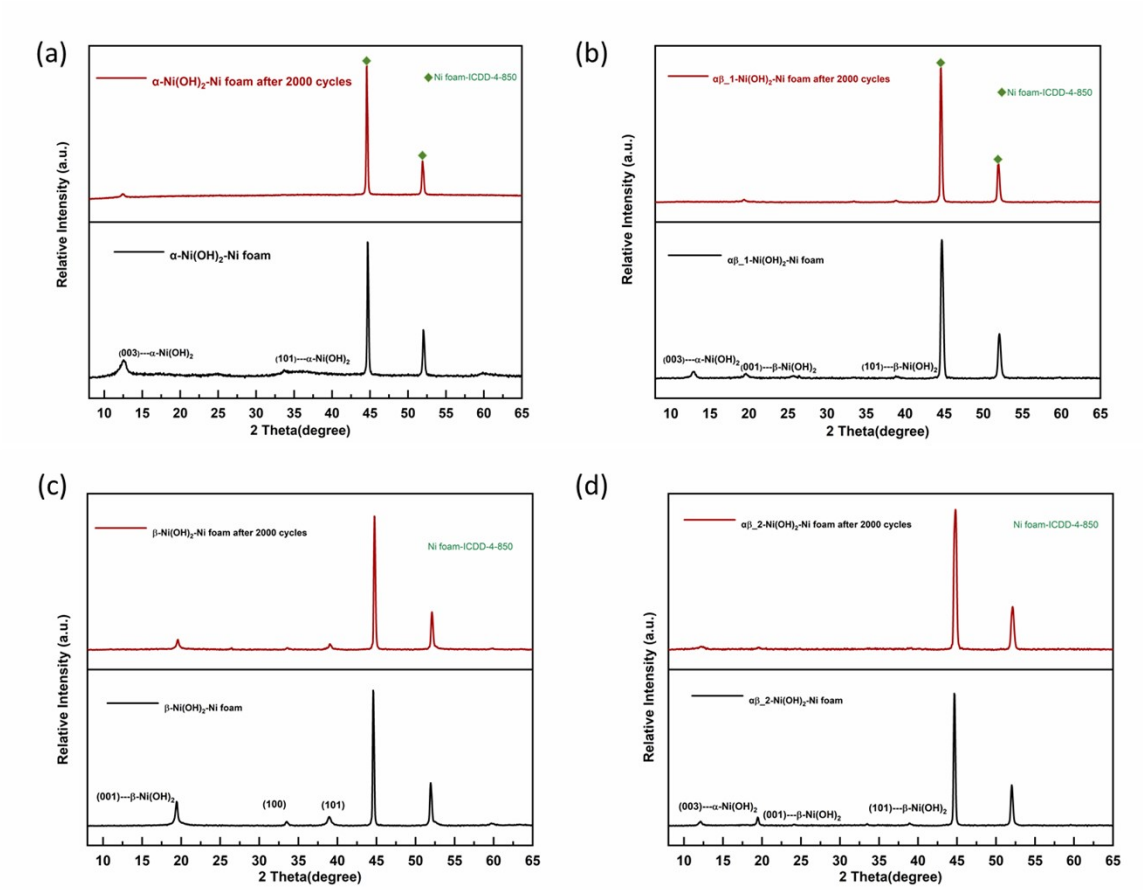

Figure S1. PXRD patterns of electrodes of nickel hydroxide grown on nickel foam before (black line) and after (red line) electrochemical measurements.

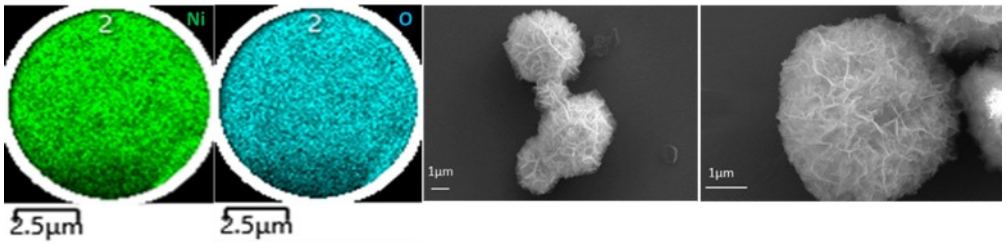

Figure S2-A. SEM images and element maps of α-Ni(OH)$_2$.

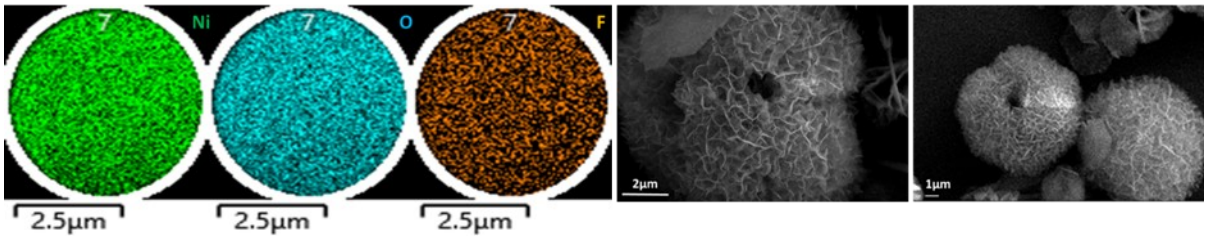

Figure S2-B. SEM images and element maps of αβ_1-Ni(OH)$_2$.

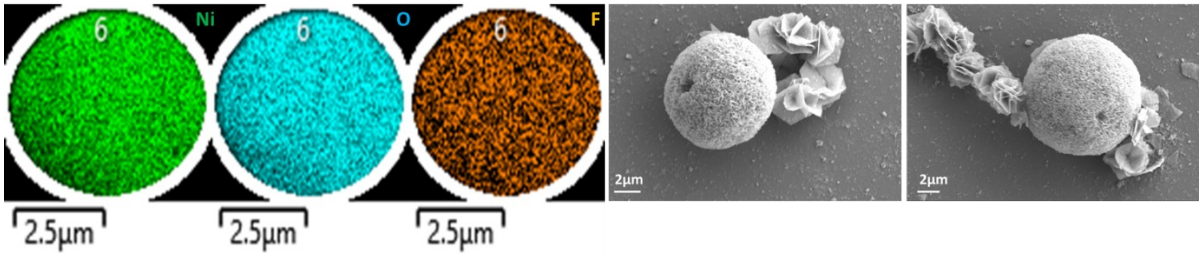

Figure S2-C. SEM images and element maps of αβ_2-Ni(OH)$_2$.

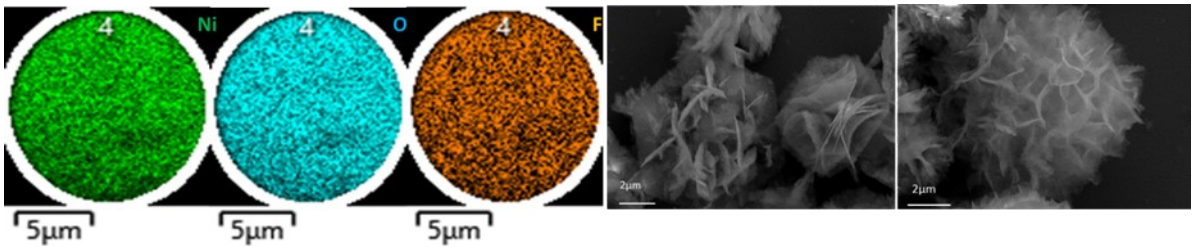

Figure S2-D. SEM images and element maps of β-Ni(OH)$_2$.

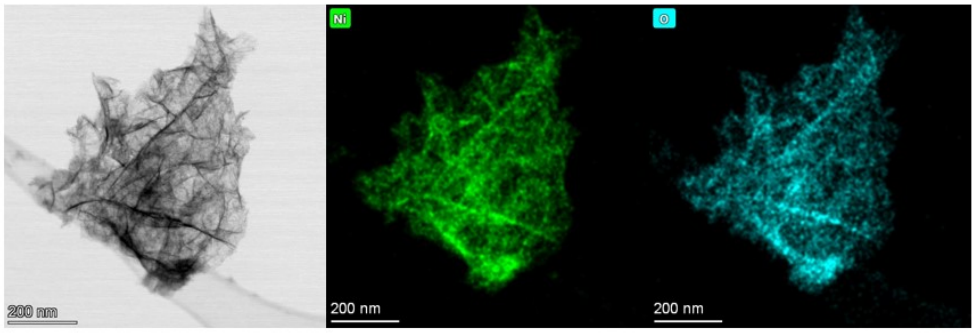

Figure S3-A. TEM image and EDS element mapping of element Ni and O of α-$Ni(OH)_2$.

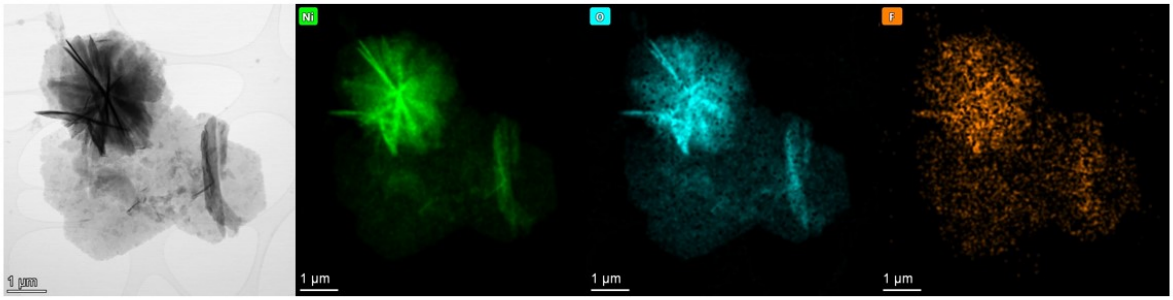

Figure S3-B. TEM image and EDS element mapping of element Ni, O and F of αβ_1-$Ni(OH)_2$.

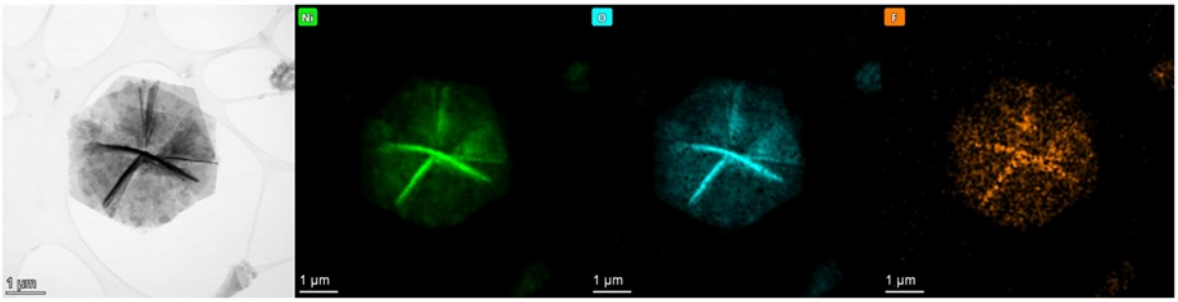

Figure S3-C. TEM image and EDS element mapping of element Ni, O and F of αβ_2-$Ni(OH)_2$.

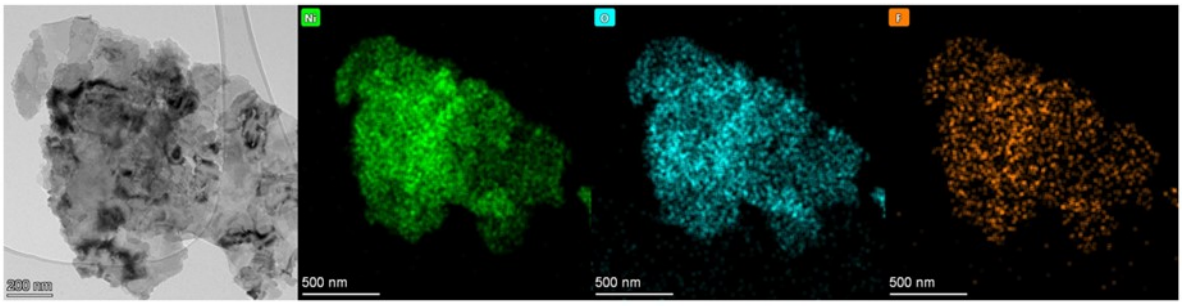

Figure S3-D. TEM image and EDS element mapping of element Ni, O and F of β-$Ni(OH)_2$.

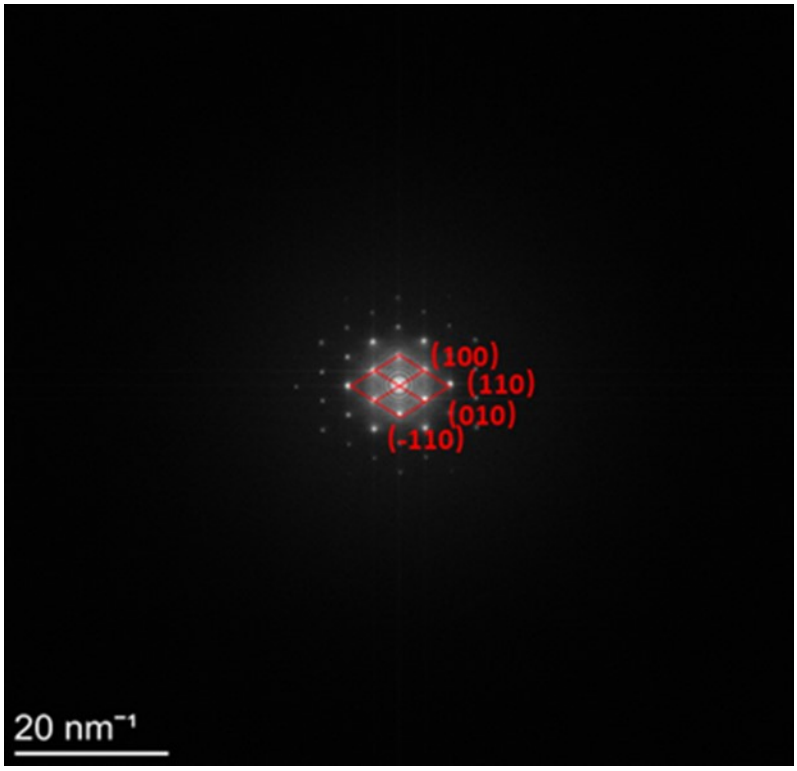

Figure S4. Fast-Fourier transform pattern (FFT) of β-$Ni(OH)_2$.

Samples name	Point	Element (Atom%)		
		O	Ni	F
α-$Ni(OH)_2$	1	67.08	32.92	----
	2	64.58	35.42	----
	3	68.79	31.21	----
	4	66.85	33.15	----
	5	70.71	29.29	----
	6	68.28	31.72	----
	Average	67.71	32.28	----
αβ_1-$Ni(OH)_2$	1	62.78	31.26	5.95
	2	62.65	31.63	5.72
	3	63.73	31.52	4.75
	4	62.07	32.21	5.71
	5	63.77	31.37	4.86
	6	59.96	34.76	5.28
	Average	62.49	32.13	5.37
Calculated ratio of F:Ni from the EDS			0.3:2	
Experimental molar ration of F:Ni			0.2:2	
αβ_2-$Ni(OH)_2$	1	60.79	31.02	8.19
	2	60.14	31.55	8.32
	3	62.57	28.88	8.88
	4	61.81	29	9.19
	5	59.92	30.02	10.06
	6	60.26	29.83	9.91
	Average	60.92	29.99	9.09
Calculated ratio of F:Ni from the EDS			0.61:2	
Experimental molar ration of F:Ni			0.5:2	
	1	56.99	30.34	12.67
β-$Ni(OH)_2$	2	56.57	31.48	11.95
	3	55.86	31.67	12.47
	4	54.93	34.14	10.93
	5	58.13	29.78	12.08
	6	57.47	29.78	10.36
	Average	56.66	31.60	11.74
Calculated ratio of F:Ni from the EDS			0.74:2	
Experimental molar ration of F:Ni			1:2	

Table S3. SEM-EDS analysis of O, Ni, F of different phases of nickel hydroxide.

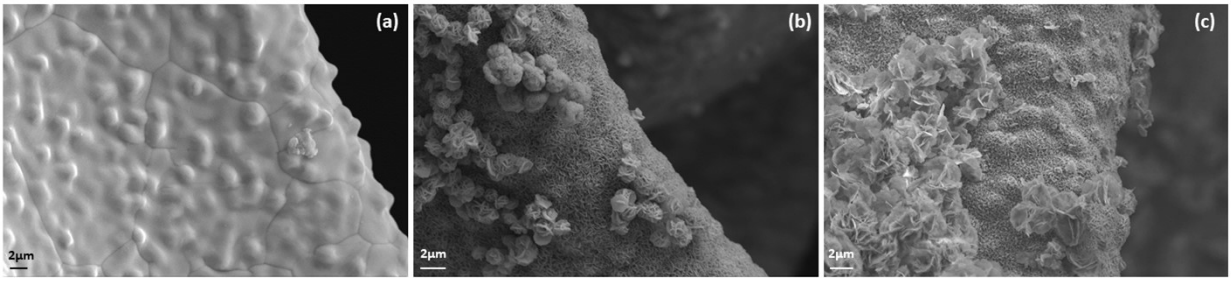

Figure S5. SEM images (a) pure nickel foam; (b) α-$Ni(OH)_2$ on nickel foam; (c) β-$Ni(OH)_2$ on nickel foam.

Assignment	Infrared band (cm^{-1})	
	α-$Ni(OH)_2$	**β-$Ni(OH)_2$**
D_{3h} nitrate stretch	835	835(very weak)
C_{2v} nitrate stretch	1053	-----
C_{2v} nitrate stretch	1280	-----
D_{3h} nitrate stretch	1370	1370
C_{2v} nitrate stretch	1500	-----
Layer H_2O (O-H bend)	1600	-----
Free H_2O (O-H bend)	1633	1633
C≡N triple bond	2213	2213
O-H stretch of α-$Ni(OH)_2$	3643	-----
Hydroxide stretch (v O-H)	-----	3626

Table S4. Infrared band assignments for α-$Ni(OH)_2$ and β-$Ni(OH)_2$.

Assignment	Raman band (cm^{-1})	
	α-$Ni(OH)_2$	**β-$Ni(OH)_2$**
Lattice mode(Ni-O)	464	464
D_{3h} nitrate stretch	1049	1049 (very weak)
C_{2v} nitrate stretch	1356	-----
C_{2v} nitrate stretch	1291	-----
H_2O	1689	-----
O-H stretch of α-$Ni(OH)_2$	3644	-----
Hydroxide stretch (v O-H)	-----	3571

Table S5. Raman band assignments for α-$Ni(OH)_2$ and β-$Ni(OH)_2$.

Sample name	α-Ni(OH)$_2$	αβ_1-Ni(OH)$_2$	αβ_2-Ni(OH)$_2$	β-Ni(OH)$_2$	Commercial
Mass loss from 25°C to 250°C	12%	10%	5%	2%	0
Mass loss from 250°C to 500°C	21%	20%	16%	15%	19%
Mass remaining above 500°C	67%	70%	79%	82%	81%

Table S6. Mass changes extracted from the TGA curves..

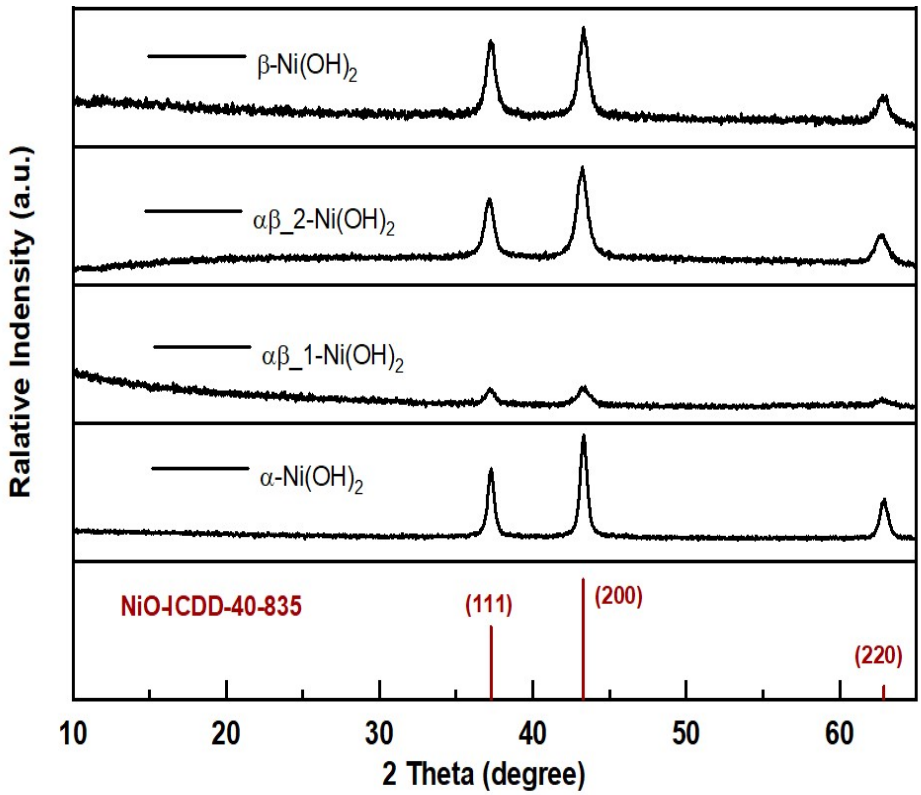

Figure S6. PXRD pattern of NiO residue after TGA

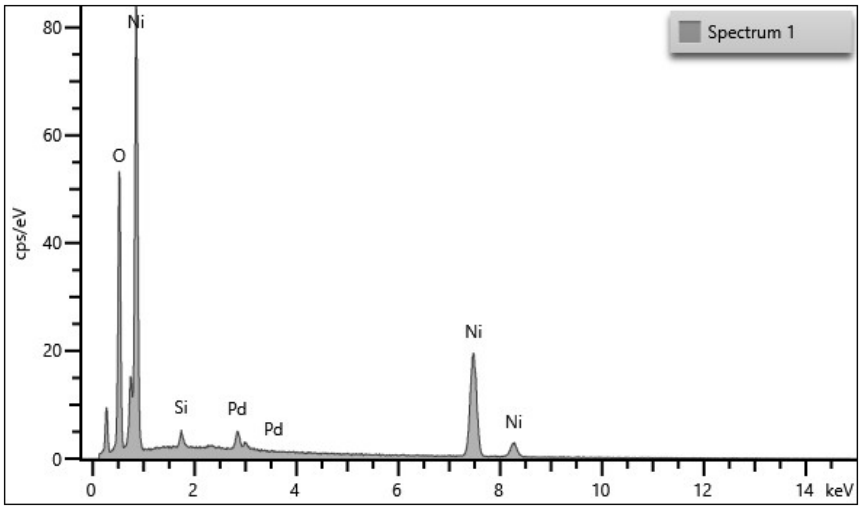

Figure S7. SEM-EDS of NiO residue after TGA (α-$Ni(OH)_2$)

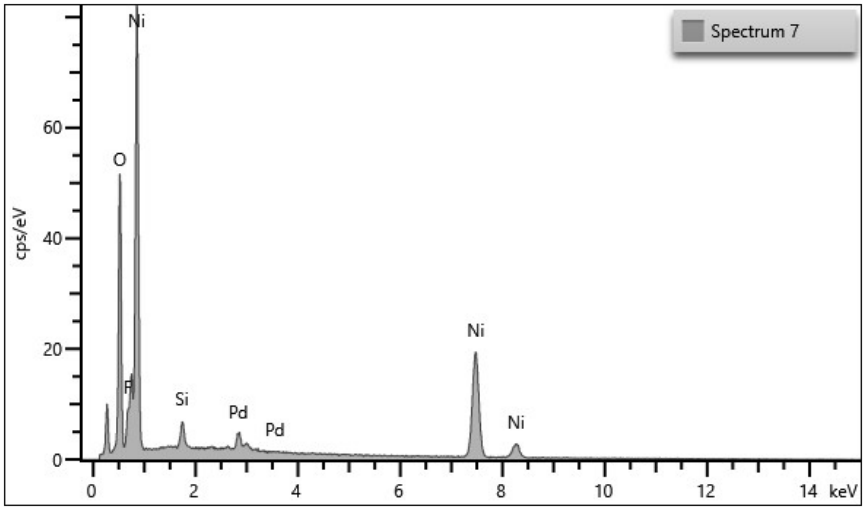

Figure S8. SEM-EDS of NiO residue after TGA (β-$Ni(OH)_2$)

Samples name	Point	Element (Atom%)		
		O	Ni	F
NiO (α-$Ni(OH)_2$)	1	48.84	51.16	----
	2	48.66	51.34	----
	3	47.97	52.03	----
	4	48.33	51.67	----
	5	49.1	50.9	----
	6	48.16	51.84	----
	Average	48.51	51.49	----
NiO (β-$Ni(OH)_2$)	1	44.11	48	7.89
	2	44.33	48.01	7.66
	3	43.13	49.78	7.09
	4	43.96	48.6	7.44
	5	42.13	51.25	6.61
	6	42.12	51.11	6.78
	Average	43.29	49.46	7.25

Table S7. SEM-EDS analysis of O, Ni, F of NiO residue after TGA (α-$Ni(OH)_2$ and β-$Ni(OH)_2$).

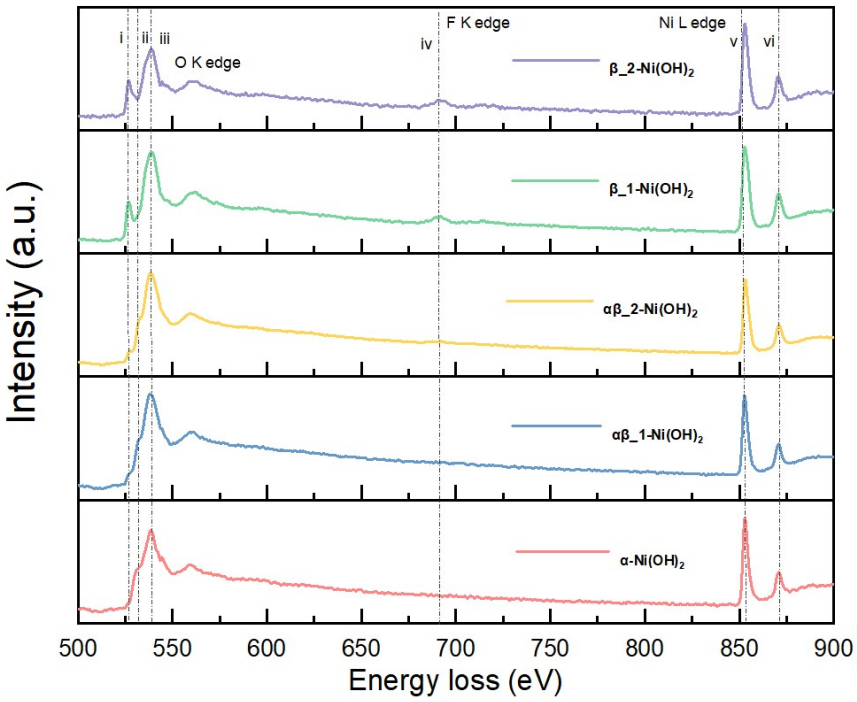

Figure S9. EELS of the oxygen and fluorine K-edge and nickel L-edge for different phases of nickel hydroxide.

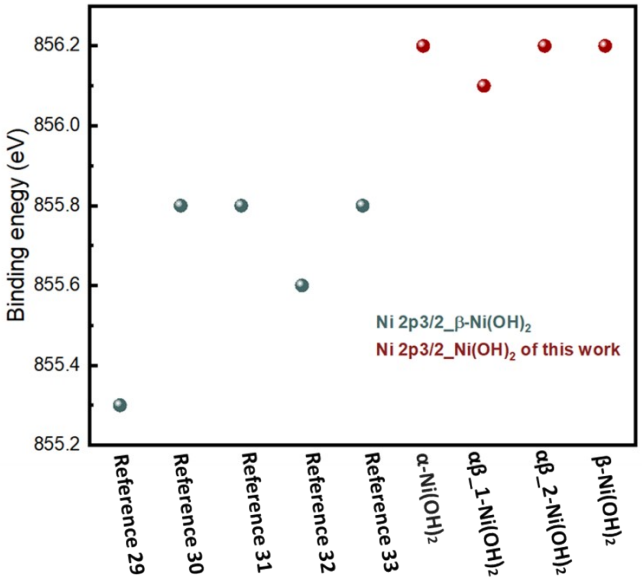

Figure S10-1. The binding energy of Ni 2p 3/2 of XPS spectrum of beta nickel hydroxide from our work (red) and published work (green).

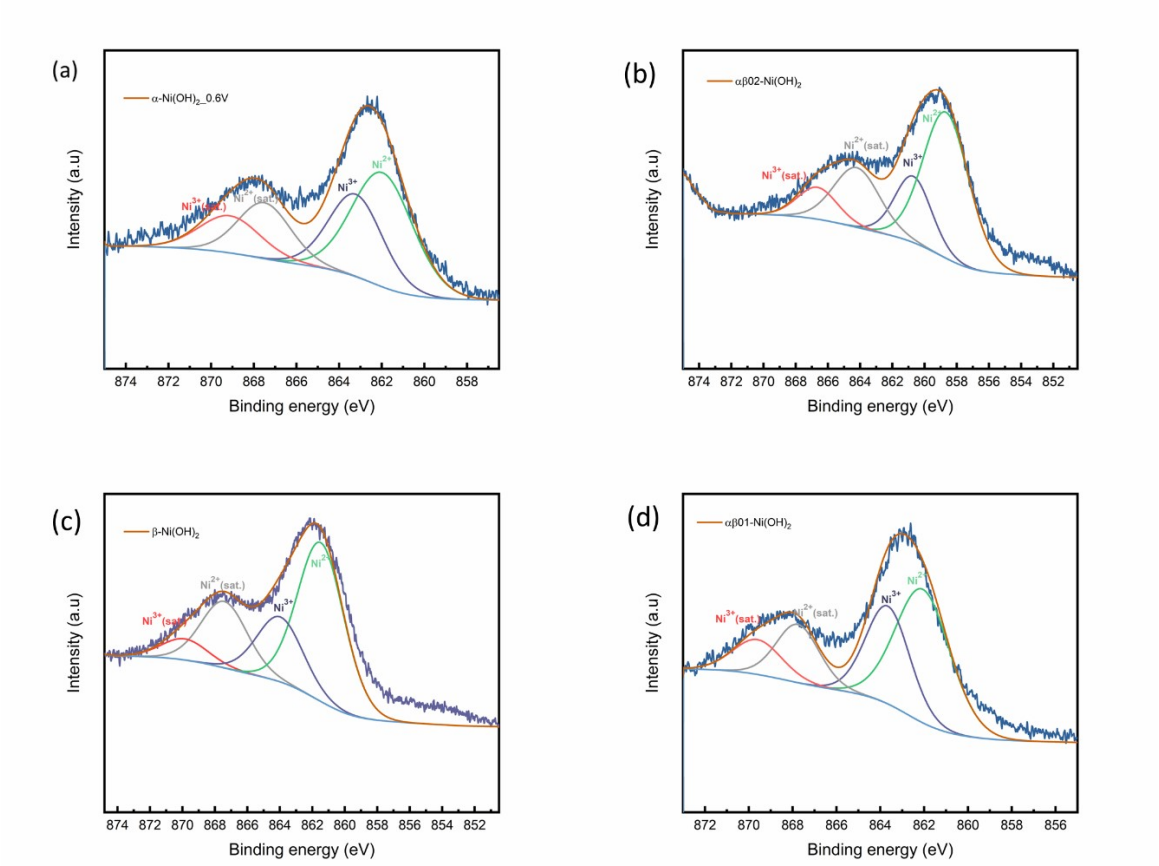

Figure S10-2. XPS Ni2p spectrum for different phases of nickel hydroxide.

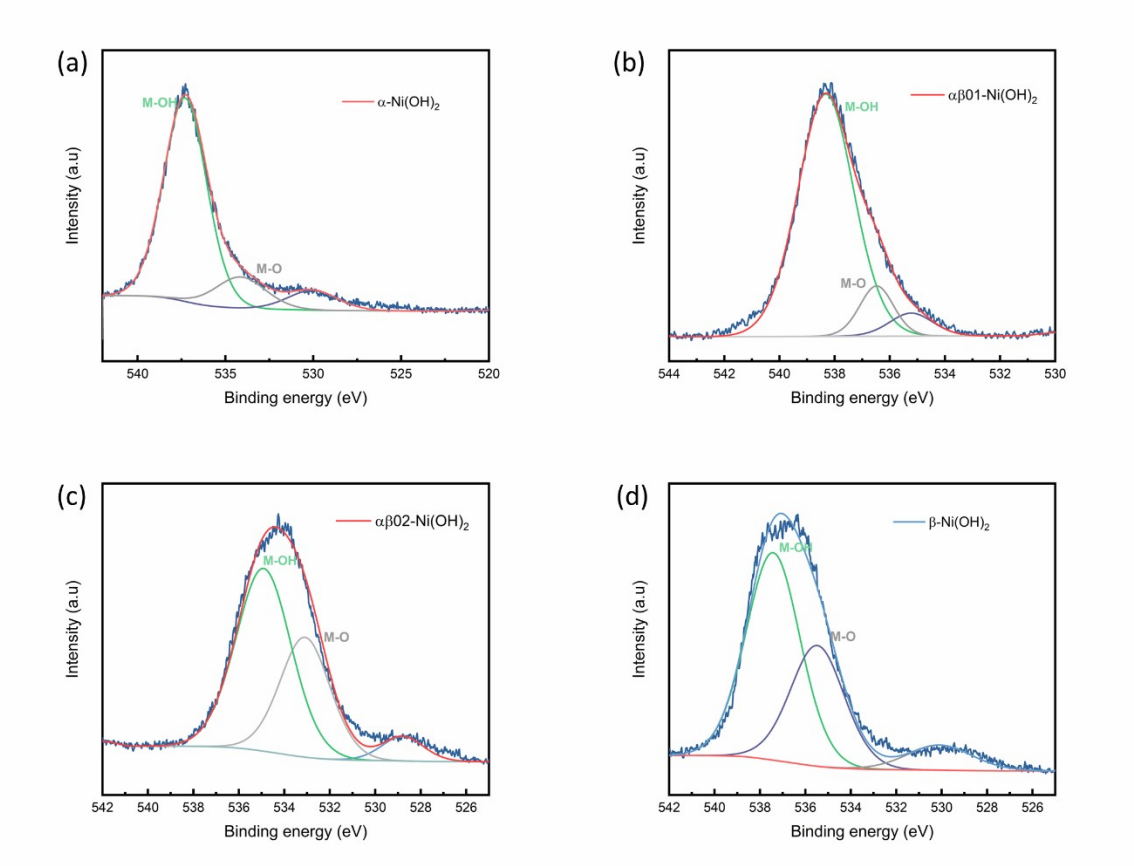

Figure S10-3. XPS Ni2p and O1s spectrum for different phases of nickel hydroxide.

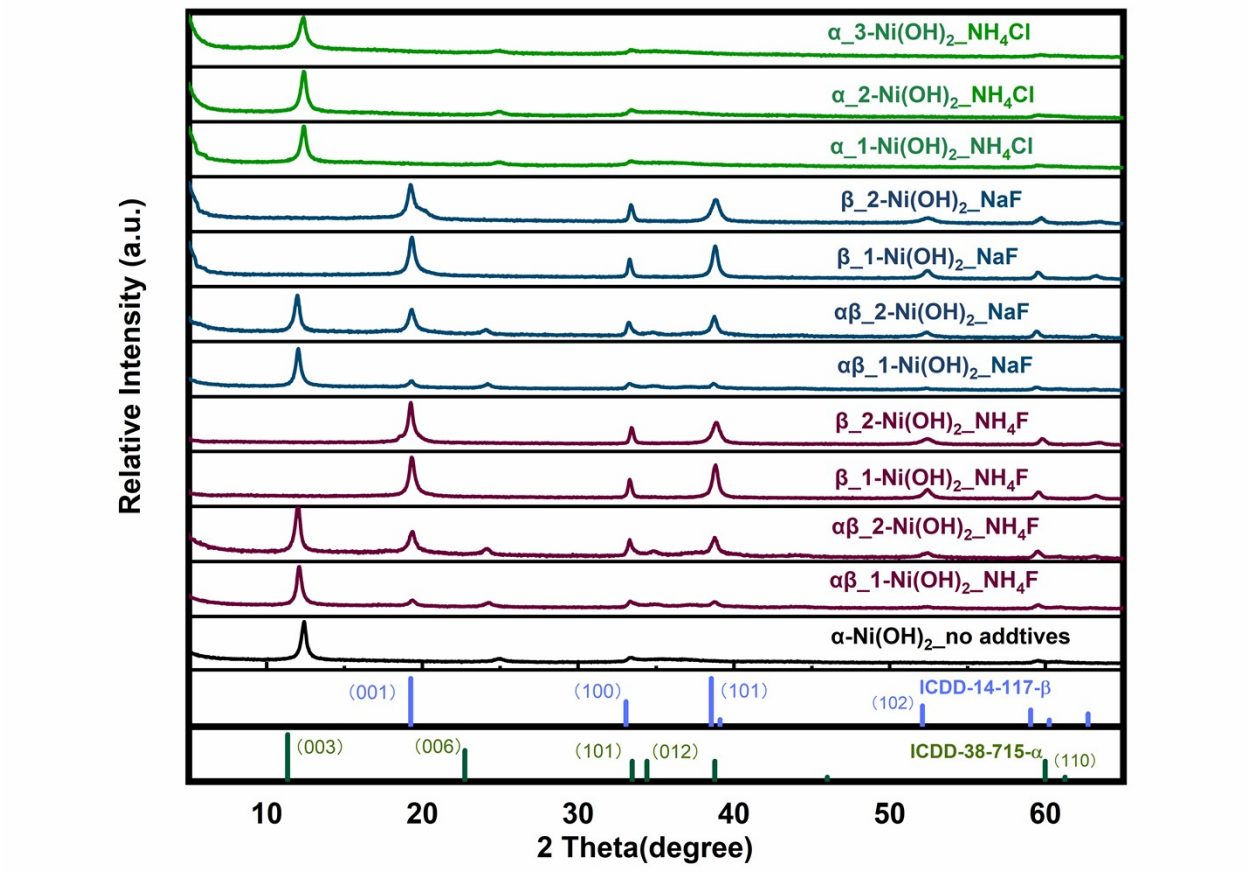

Figure S11. PXRD patterns of nickel hydroxide powder prepared with different additives.

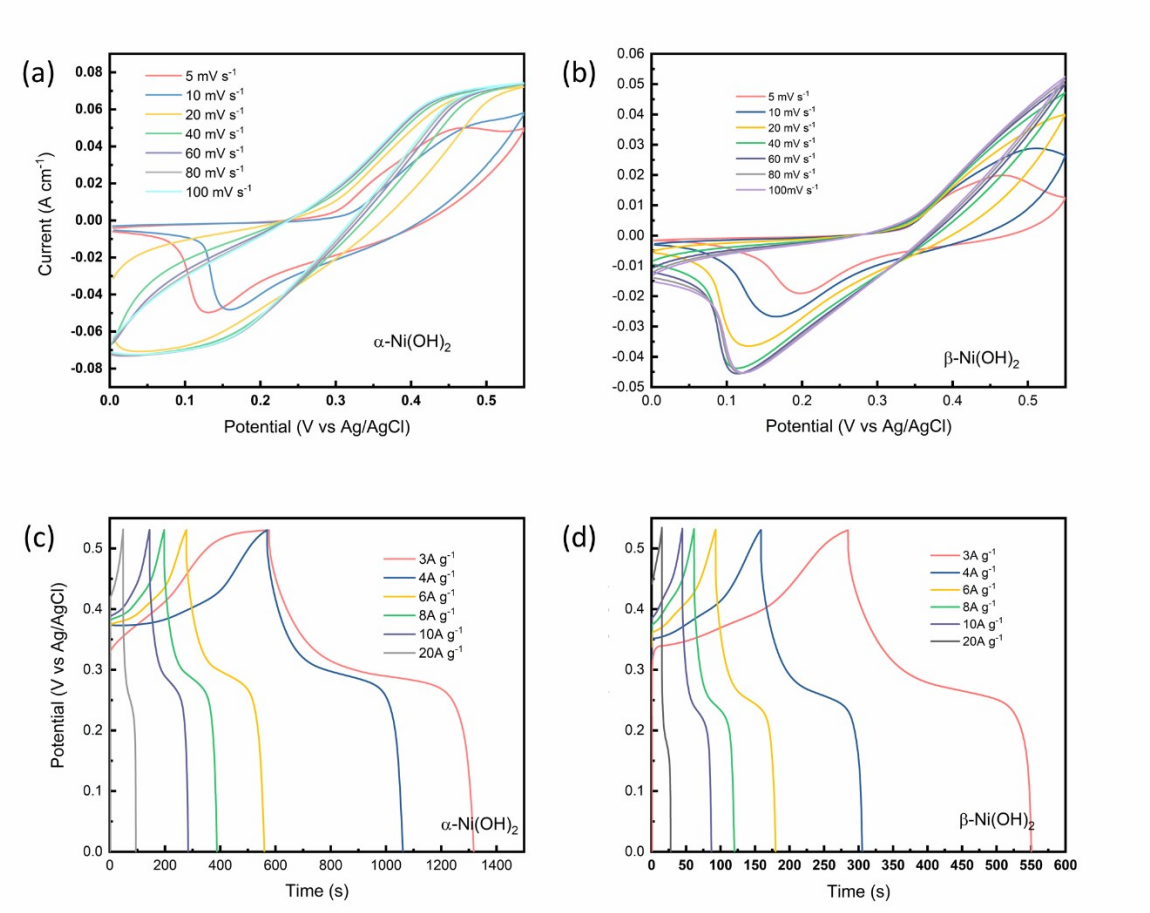

Figure S12. (a-c) CV curves of α-$Ni(OH)_2$ and β-$Ni(OH)_2$ at different scan rates. (d-f) Galvanostatic charge-discharge curves of α-$Ni(OH)_2$ and β-$Ni(OH)_2$ at various current densities.

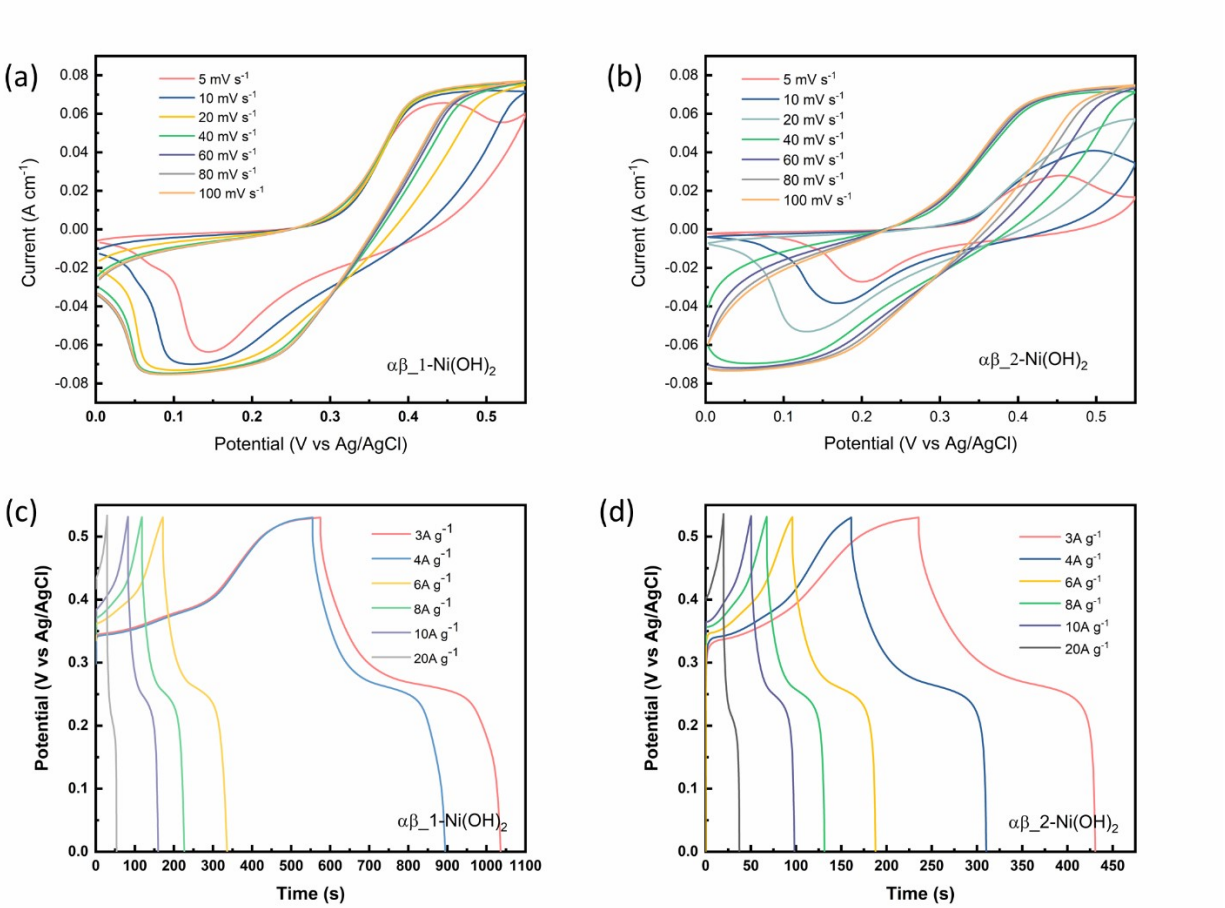

Figure S13. (a-b) CV curves of αβ_1-Ni(OH)$_2$ and αβ_2-Ni(OH)$_2$ at different scan rates. (c-d) Galvanostatic charge-discharge curves of αβ_1-Ni(OH)$_2$ and αβ_2-Ni(OH)$_2$ at various current densities.

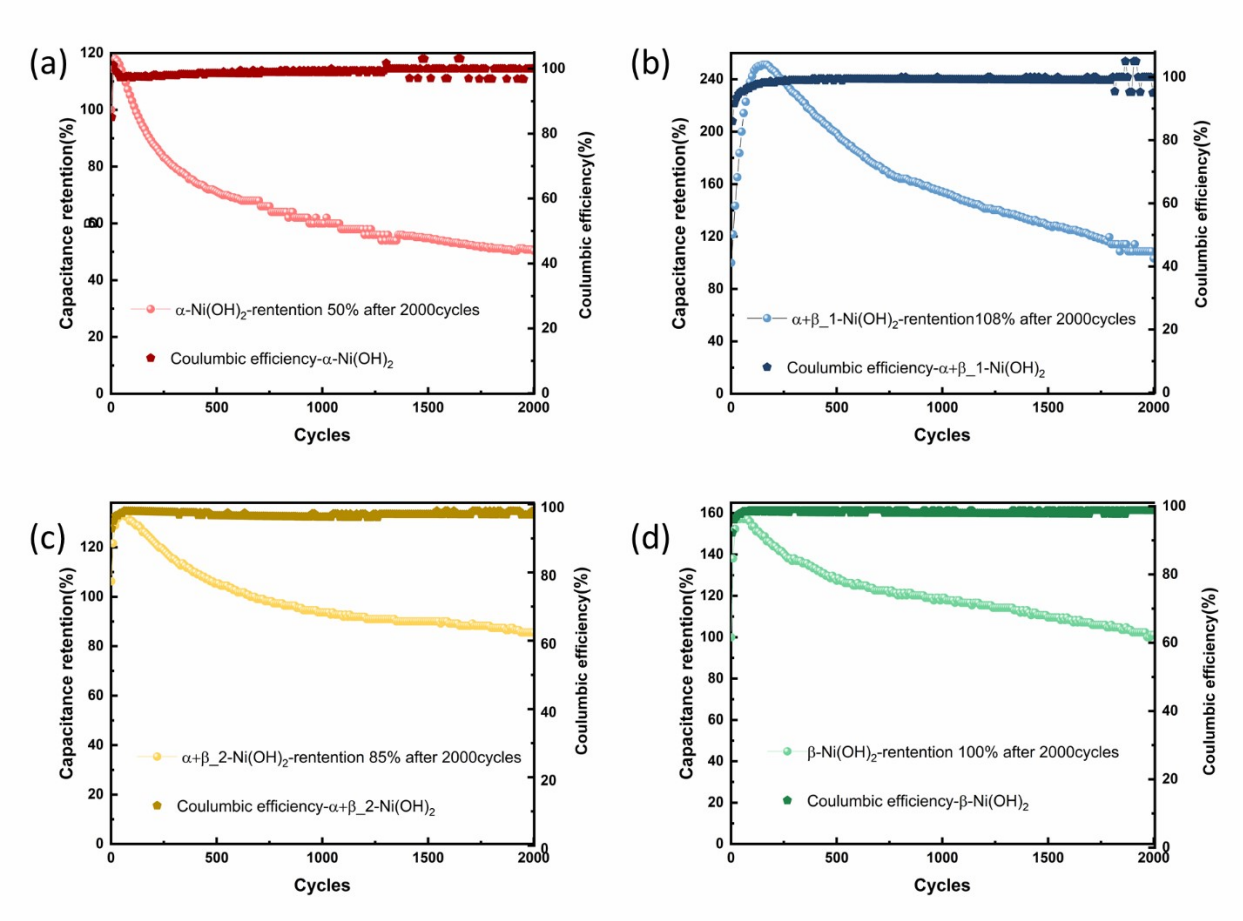

Figure S14. Cycling stability and Coulombic efficiency during cycling of (a) α-$Ni(OH)_2$; (b) αβ_1-$Ni(OH)_2$; (c) αβ_2-$Ni(OH)_2$; (d) β-$Ni(OH)_2$.

Sample	R1(RS)	R2(Rct)	ESR (RS+Rct)	Chi-Squared
α-$Ni(OH)_2$	1.3	0.76	2.06	4.3×10^{-4}
αβ_1-$Ni(OH)_2$	1.04	0.89	1.93	5.0×10^{-4}
αβ_2-$Ni(OH)_2$	1.11	1.12	2.23	1.6×10^{-3}
β-$Ni(OH)_2$	0.87	1.73	2.60	2.8×10^{-3}

Table S8. Fitting parameters for the equivalent circuit model.

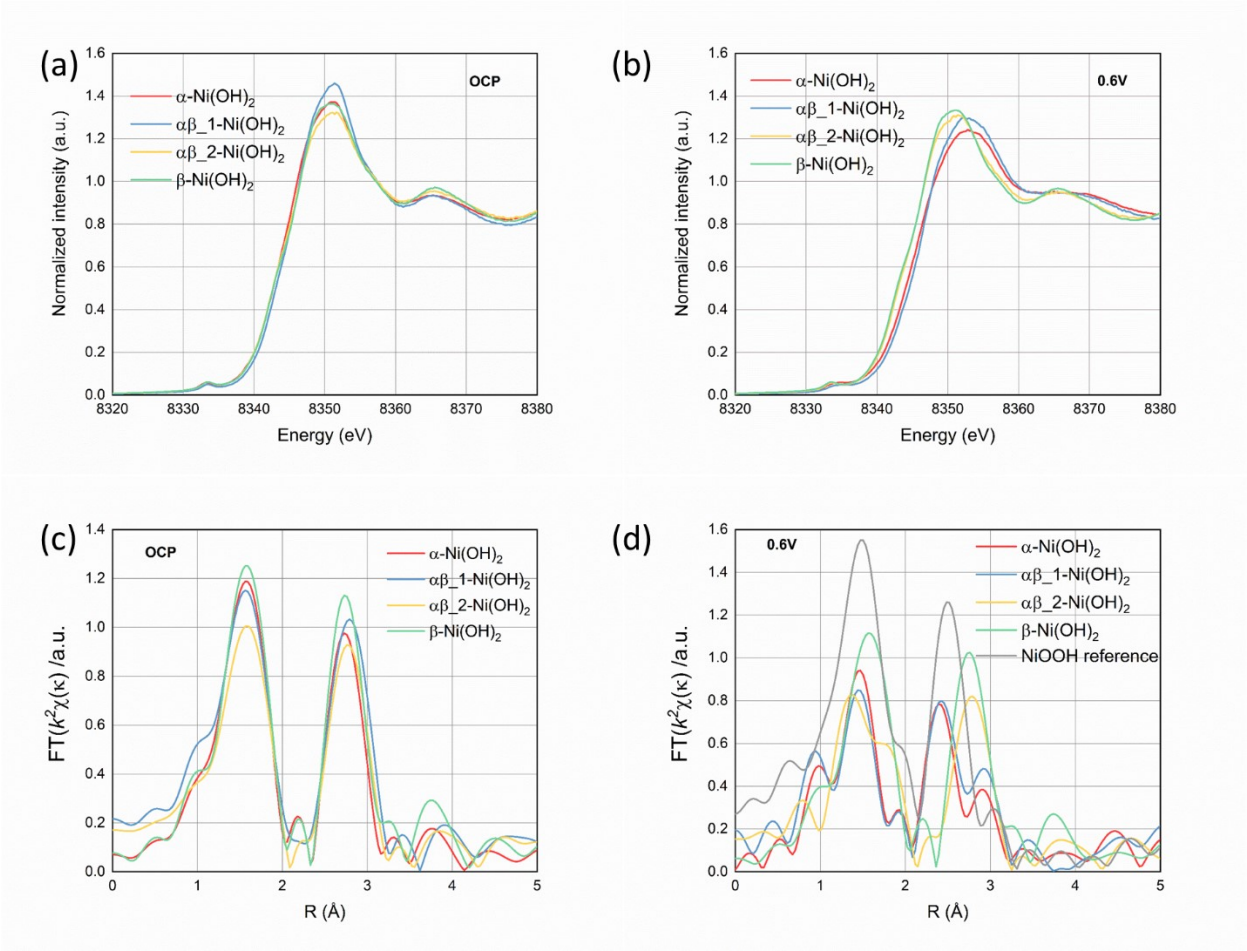

Figure S15 (a-b) Normalized Ni-edge XANES spectra under open circuit potential (OCP) and 0.6V for different nickel hydroxide samples. (c-d) The FT signal of the K^2-weighted EXAFS under OCP and 0.6V for different nickel hydroxide samples.

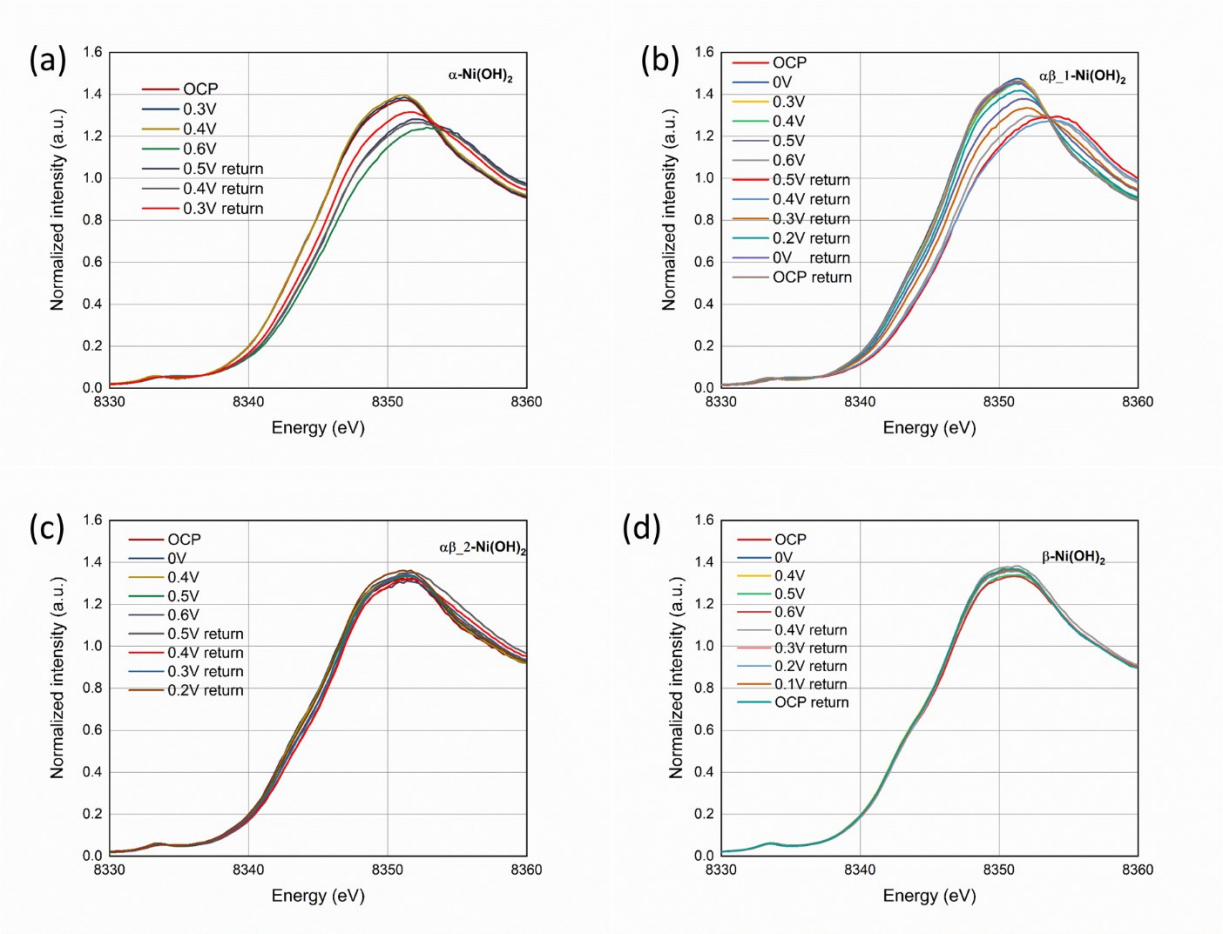

Figure S16 Enlarged normalized Ni-edge XANES spectra under different potential of (a) α-$Ni(OH)_2$; (b) αβ_1-$Ni(OH)_2$; (c) αβ_2-$Ni(OH)_2$; (d) β-$Ni(OH)_2$.

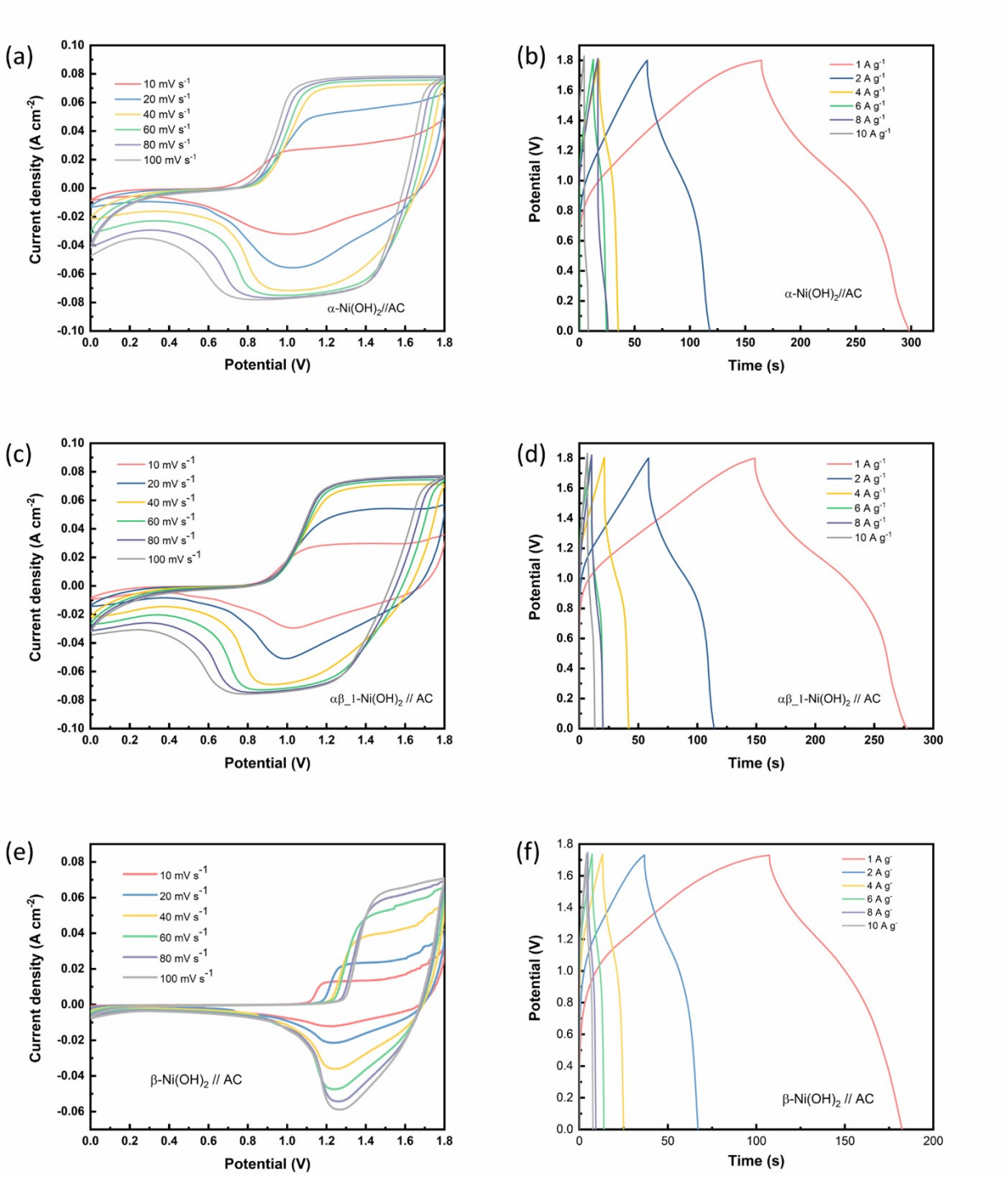

Figure S17. (a-b) CV and GCD curves of the α-$Ni(OH)_2$ //AC hybrid-supercapacitor. (c-d) CV and GCD curves of the αβ_1-$Ni(OH)_2$ //AC hybrid-supercapacitor. (e-f) CV and GCD curves of the β-$Ni(OH)_2$ //AC hybrid-supercapacitor.

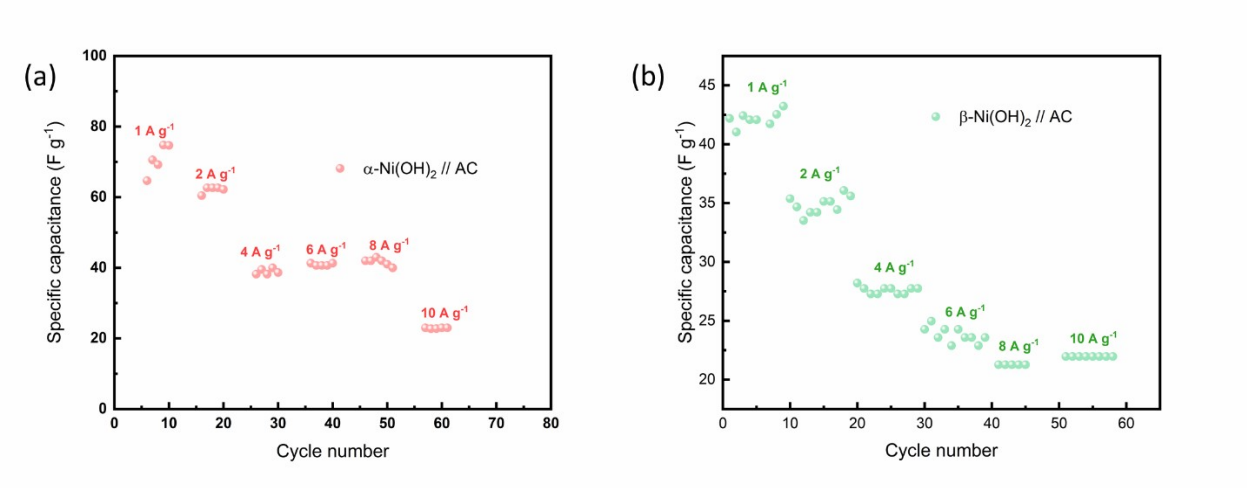

Figure S18. The specific capacitance evolution under various current densities of (a) α-$Ni(OH)_2$//AC. (b) β-$Ni(OH)_2$ //AC hybrid-supercapacitor.

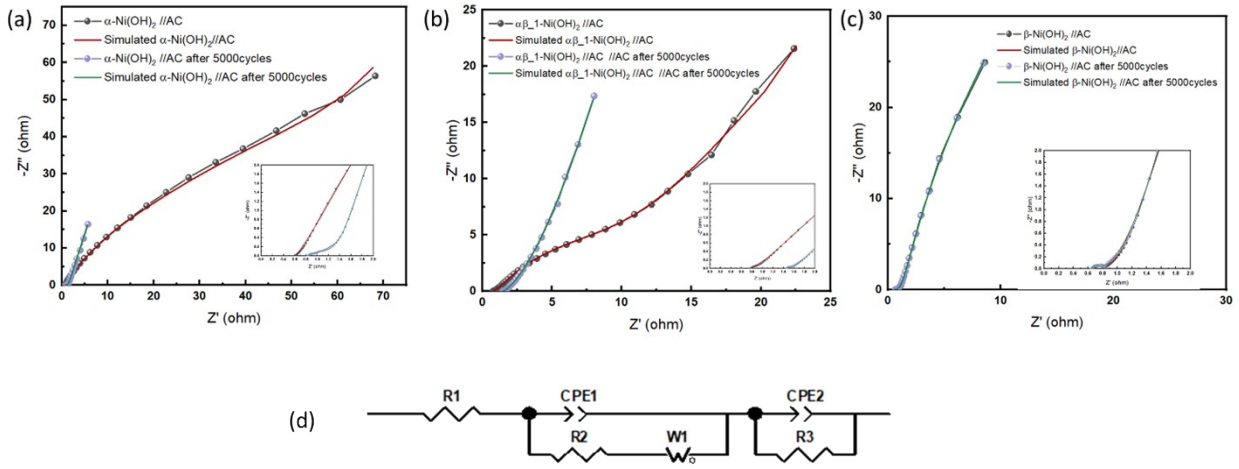

Figure S19. Nyquist plots, inset show the enlarged figures the in two-electrode configuration of (a) α-$Ni(OH)_2$ //AC, (b) αβ_1-$Ni(OH)_2$//AC, (c) β_1-$Ni(OH)_2$ //AC. (d) The corresponding equivalent circuit.

α-$Ni(OH)_2$ (Two-electrode potential window: 1.8V)	Three-electrode configuration (Electrode mass:2.8 mg cm^{2-})	Current density (A g^{-1})	3	4	6	8	10	20	---
		Capacity (C g-1)	2223	1970	1710	1531	1400	936	---
		Scan rate (mV s^{-1})	5	10	20	40	60	80	100
		Capacitance (F g^{-1})	987	428	317	128	80	57	44
	Two-electrode configuration (α-$Ni(OH)_2$//AC, total electrodes mass: ~20mg)	Current density (A g^{-1})	1	2	4	6	8	10	
		Capacitance (F g^{-1})	75	63	40	41	40	23	
		Energy density (Wh kg^{-1})	34	28	18	19	18	11	
		Power density (W kg^{-1})	900	1800	3600	5400	7200	9000	
$\alpha\beta$ _1-$Ni(OH)_2$ (Two-electrode potential window: 1.8V)	Three-electrode configuration (Electrode mass:2.1 mg cm^{2-})	Current density	3	4	6	8	10	20	---
		Capacity	1396	1368	1000	890	778	500	---
		Scan rate	5	10	20	40	60	80	100
		Capacitance	1790	1049	504	242	161	120	94
	Two-electrode configuration ($\alpha\beta$ _1-$Ni(OH)_2$//AC total electrodes mass: ~ 17 mg)	Current density	1	2	4	6	8	10	
		Capacitance	71	62	47	33	45	37	
		Energy density	32	28	21	15	20	17	
		Power density	900	1800	3600	5400	7200	9000	
$\alpha\beta$ _2-$Ni(OH)_2$	Three-electrode configuration (Electrode mass:3.0 mg cm^{2-})	Current density	3	4	6	8	10	20	---
		Capacity	587	608	551	512	489	348	---
		Scan rate	5	10	20	40	60	80	100
		Capacitance	498	357	213	177	109	77	59
β-$Ni(OH)_2$ (Two-electrode potential window: 1.73V)	Three-electrode configu(electrode mass:2.2 mg cm^{2-})ration	Current density	3	4	6	8	10	20	---
		Capacity	797	588	517	467	422	226	---
		Scan rate	5	10	20	40	60	80	100
		Capacitance	485	327	187	97	65	48	38
	Two-electrode configuration (β _1-$Ni(OH)_2$//AC, total electrodes mass: ~ 13mg)	Current density	1	2	4	6	8	10	
		Capacitance	43	36	28	24	22	22	
		Energy density	18	15	12	10	9	9	
		Power density	865	1730	3460	5190	6920	8650	

Table S9. Electrochemical performance of nickel hydroxide electrodes in three-electrode configurations and two-electrode configurations.